




# Erratum to: Determination of the strong coupling constant $\alpha_s(m_Z)$ in next-to-next-to-leading order QCD using H1 jet cross section measurements

## H1 Collaboration

V. Andreev<sup>19</sup>, A. Bagdasaryan<sup>31</sup>, K. Begzsuren<sup>28</sup>, A. Belousov<sup>19</sup>, V. Bertone<sup>46,47\*</sup>, A. Bolz<sup>12</sup>, V. Boudry<sup>22</sup>, G. Brandt<sup>41</sup>, V. Brisson<sup>21</sup>, D. Britzger<sup>12</sup>, A. Buniatian<sup>2</sup>, A. Bylinkin<sup>43</sup>, L. Bystritskaya<sup>18</sup>, A. J. Campbell<sup>10</sup>, K. B. Cantun Avila<sup>17</sup>, K. Cerny<sup>25</sup>, V. Chekelian<sup>20</sup>, J. G. Contreras<sup>17</sup>, J. Cvach<sup>24</sup>, J. Currie<sup>48,\*</sup>, J. B. Dainton<sup>14</sup>, K. Daum<sup>30</sup>, C. Diaconu<sup>16</sup>, M. Dobre<sup>4</sup>, V. Dodonov<sup>10,†</sup>, G. Eckerlin<sup>10</sup>, S. Egli<sup>29</sup>, E. Elsen<sup>10</sup>, L. Favart<sup>3</sup>, A. Fedotov<sup>18</sup>, J. Feltesse<sup>9</sup>, M. Fleischer<sup>10</sup>, A. Fomenko<sup>19</sup>, E. Gabathuler<sup>14,†</sup>, J. Gayler<sup>10</sup>, T. Gehrman<sup>34,\*</sup>, S. Ghazaryan<sup>10,†</sup>, L. Goerlich<sup>6</sup>, N. Gogitidze<sup>19</sup>, M. Gouzevitch<sup>35</sup>, C. Grab<sup>33</sup>, A. Grebenyuk<sup>3</sup>, T. Greenshaw<sup>14</sup>, G. Grindhammer<sup>20</sup>, C. Gwenlan<sup>44,\*</sup>, D. Haidt<sup>10</sup>, R. C. W. Henderson<sup>13</sup>, J. Hladký<sup>24</sup>, D. Hoffmann<sup>16</sup>, R. Horisberger<sup>29</sup>, T. Hreus<sup>3</sup>, F. Huber<sup>12</sup>, A. Huss<sup>33,\*</sup>, M. Jacquet<sup>21</sup>, X. Janssen<sup>3</sup>, A. W. Jung<sup>45</sup>, H. Jung<sup>10</sup>, M. Kapichine<sup>8</sup>, J. Katzy<sup>10</sup>, C. Kiesling<sup>20</sup>, M. Klein<sup>14</sup>, C. Kleinwort<sup>10</sup>, R. Kogler<sup>11</sup>, P. Kostka<sup>14</sup>, J. Kretzschmar<sup>14</sup>, D. Krücker<sup>10</sup>, K. Krüger<sup>10</sup>, M. P. J. Landon<sup>15</sup>, W. Lange<sup>32</sup>, P. Laycock<sup>14</sup>, A. Lebedev<sup>19</sup>, S. Levonian<sup>10</sup>, K. Lipka<sup>10</sup>, B. List<sup>10</sup>, J. List<sup>10</sup>, B. Lobodzinski<sup>20</sup>, E. Malinovski<sup>19</sup>, H.-U. Martyn<sup>1</sup>, S. J. Maxfield<sup>14</sup>, A. Mehta<sup>14</sup>, A. B. Meyer<sup>10</sup>, H. Meyer<sup>30</sup>, J. Meyer<sup>10</sup>, S. Mikocki<sup>6</sup>, A. Morozov<sup>8</sup>, K. Müller<sup>34</sup>, Th. Naumann<sup>32</sup>, P. R. Newman<sup>2</sup>, C. Niebuhr<sup>10</sup>, J. Niehues<sup>34,\*</sup>, G. Nowak<sup>6</sup>, J. E. Olsson<sup>10</sup>, D. Ozerov<sup>29</sup>, C. Pascaud<sup>21</sup>, G. D. Patel<sup>14</sup>, E. Perez<sup>37</sup>, A. Petrukhin<sup>35</sup>, I. Picuric<sup>23</sup>, H. Pirumov<sup>10</sup>, D. Pitzl<sup>10</sup>, R. Plačakyte<sup>10</sup>, R. Polifka<sup>25,39</sup>, K. Rabbertz<sup>49,\*</sup>, V. Radescu<sup>44</sup>, N. Raicevic<sup>23</sup>, T. Ravdandorj<sup>28</sup>, P. Reimer<sup>24</sup>, E. Rizvi<sup>15</sup>, P. Robmann<sup>34</sup>, R. Roosen<sup>3</sup>, A. Rostovtsev<sup>42</sup>, M. Rotaru<sup>4</sup>, D. Šálek<sup>25</sup>, D. P. C. Sankey<sup>5</sup>, M. Sauter<sup>12</sup>, E. Sauvan<sup>16,40</sup>, S. Schmitt<sup>10,a</sup> , L. Schoeffel<sup>9</sup>, A. Schöning<sup>12</sup>, F. Sefkow<sup>10</sup>, S. Shushkevich<sup>36</sup>, Y. Soloviev<sup>19</sup>, P. Sopicki<sup>6</sup>, D. South<sup>10</sup>, V. Spaskov<sup>8</sup>, A. Specka<sup>22</sup>, M. Steder<sup>10</sup>, B. Stella<sup>26</sup>, U. Straumann<sup>34</sup>, M. R. Sutton<sup>50,\*</sup>, T. Sykora<sup>3,25</sup>, P. D. Thompson<sup>2</sup>, D. Traynor<sup>15</sup>, P. Truöl<sup>34,†</sup>, I. Tsakov<sup>27</sup>, B. Tseepeldorj<sup>28,38</sup>, A. Valkárová<sup>25</sup>, C. Vallée<sup>16</sup>, P. Van Mechelen<sup>3</sup>, Y. Vazdik<sup>19,†</sup>, D. Wegener<sup>7</sup>, E. Wunsch<sup>10</sup>, J. Žáček<sup>25</sup>, Z. Zhang<sup>21</sup>, R. Žlebčík<sup>10</sup>, H. Zohrabyan<sup>31</sup>, F. Zomer<sup>21</sup>

<sup>1</sup> I. Physikalisches Institut der RWTH, Aachen, Germany<sup>2</sup> School of Physics and Astronomy, University of Birmingham, Birmingham, UK<sup>c</sup><sup>3</sup> Inter-University Institute for High Energies ULB-VUB, Brussels and Universiteit Antwerpen, Antwerp, Belgium<sup>d</sup><sup>4</sup> Horia Hulubei National Institute for R&D in Physics and Nuclear Engineering (IFIN-HH), Bucharest, Romania<sup>d</sup><sup>5</sup> STFC, Rutherford Appleton Laboratory, Didcot, Oxfordshire, UK<sup>c</sup><sup>6</sup> Institute of Nuclear Physics, Polish Academy of Sciences, 31342 Kraków, Poland<sup>e</sup><sup>7</sup> Institut für Physik, TU Dortmund, Dortmund, Germany<sup>b</sup><sup>8</sup> Joint Institute for Nuclear Research, Dubna, Russia<sup>9</sup> Irfu/SPP, CE Saclay, Gif-sur-Yvette, France<sup>10</sup> DESY, Hamburg, Germany<sup>11</sup> Institut für Experimentalphysik, Universität Hamburg, Hamburg, Germany<sup>b</sup><sup>12</sup> Physikalisches Institut, Universität Heidelberg, Heidelberg, Germany<sup>b</sup><sup>13</sup> Department of Physics, University of Lancaster, Lancaster, UK<sup>c</sup><sup>14</sup> Department of Physics, University of Liverpool, Liverpool, UK<sup>c</sup><sup>15</sup> School of Physics and Astronomy, Queen Mary University of London, London, UK<sup>c</sup><sup>16</sup> Aix Marseille Université, CNRS/IN2P3, CPPM UMR 7346, 13288 Marseille, France<sup>17</sup> Departamento de Física Aplicada, CINVESTAV, Mérida, Yucatán, Mexico<sup>b</sup><sup>18</sup> Institute for Theoretical and Experimental Physics, Moscow, Russia<sup>d</sup><sup>19</sup> Lebedev Physical Institute, Moscow, Russia<sup>20</sup> Max-Planck-Institut für Physik, Munich, Germany<sup>21</sup> LAL, Université Paris-Sud, CNRS/IN2P3, Orsay, France<sup>22</sup> LLR, Ecole Polytechnique, CNRS/IN2P3, Palaiseau, France<sup>23</sup> Faculty of Science, University of Montenegro, Podgorica, Montenegro<sup>k</sup><sup>24</sup> Institute of Physics, Academy of Sciences of the Czech Republic, Prague, Czech Republic<sup>f</sup><sup>25</sup> Faculty of Mathematics and Physics, Charles University, Prague, Czech Republic<sup>f</sup><sup>26</sup> Dipartimento di Fisica, Università di Roma Tre and INFN Roma 3, Rome, Italy

- <sup>27</sup> Institute for Nuclear Research and Nuclear Energy, Sofia, Bulgaria  
<sup>28</sup> Institute of Physics and Technology of the Mongolian Academy of Sciences, Ulaanbaatar, Mongolia  
<sup>29</sup> Paul Scherrer Institute, Villigen, Switzerland  
<sup>30</sup> Fachbereich C, Universität Wuppertal, Wuppertal, Germany  
<sup>31</sup> Yerevan Physics Institute, Yerevan, Armenia  
<sup>32</sup> DESY, Zeuthen, Germany  
<sup>33</sup> Institut für Teilchenphysik, ETH Zürich, Zurich, Switzerland<sup>g</sup>  
<sup>34</sup> Physik-Institut der Universität Zürich, Zurich, Switzerland<sup>g</sup>  
<sup>35</sup> Now at IPNL, Université Claude Bernard Lyon 1, CNRS/IN2P3, Villeurbanne, France  
<sup>36</sup> Now at Skobeltsyn Institute of Nuclear Physics, Lomonosov Moscow State University, Moscow, Russia  
<sup>37</sup> Now at CERN, Geneva, Switzerland  
<sup>38</sup> Also at Ulaanbaatar University, Ulaanbaatar, Mongolia  
<sup>39</sup> Also at Department of Physics, University of Toronto, Toronto, ON M5S 1A7, Canada  
<sup>40</sup> Also at LAPP, Université de Savoie, CNRS/IN2P3, Annecy-le-Vieux, France  
<sup>41</sup> Now at II. Physikalisches Institut, Universität Göttingen, Göttingen, Germany  
<sup>42</sup> Now at Institute for Information Transmission Problems RAS, Moscow, Russia<sup>l</sup>  
<sup>43</sup> Now at Moscow Institute of Physics and Technology, Dolgoprudny, Moscow Region, Russian Federation<sup>m</sup>  
<sup>44</sup> Now at Department of Physics, Oxford University, Oxford, UK  
<sup>45</sup> Now at Department of Physics and Astronomy, Purdue University, 525 Northwestern Ave, West Lafayette, IN 47907, USA  
<sup>46</sup> Department of Physics and Astronomy, Vrije University, De Boelelaan, 1081 Amsterdam, The Netherlands  
<sup>47</sup> National Institute for Subatomic Physics (NIKHEF), Science Park 105, Amsterdam, The Netherlands  
<sup>48</sup> Institute for Particle Physics Phenomenology, Ogden Centre for Fundamental Physics, Durham University, South Road, Durham, UK  
<sup>49</sup> Karlsruher Institut für Technologie (KIT), Institut für Experimentelle Teilchenphysik (ETP), Wolfgang-Gaede-Str. 1, Karlsruhe, Germany  
<sup>50</sup> Department of Physics and Astronomy, University of Sussex, Pevensey II, Brighton, UK

Received: 16 June 2021 / Accepted: 28 June 2021

© The Author(s) 2021

**Abstract** The determination of the strong coupling constant  $\alpha_s(m_Z)$  from H1 inclusive and dijet cross section data [1] exploits perturbative QCD predictions in next-to-next-to-leading order (NNLO) [2–4]. An implementation

The original article can be found online at <https://doi.org/10.1140/epjc/s10052-017-5314-7>.

<sup>a</sup> e-mail: [sschmitt@mail.desy.de](mailto:sschmitt@mail.desy.de)

<sup>†</sup> Deceased

<sup>\*</sup> Contributing author providing theory predictions or infrastructure

<sup>b</sup> Supported by the Bundesministerium für Bildung und Forschung, FRG, under contract numbers 05H09GUF, 05H09VHC, 05H09VHF, 05H16PEA

<sup>c</sup> Supported by the UK Science and Technology Facilities Council, and formerly by the UK Particle Physics and Astronomy Research Council

<sup>d</sup> Supported by FNRS-FWO-Vlaanderen, IISN-IKW and IWT and by Interuniversity Attraction Poles Programme, Belgian Science Policy

<sup>e</sup> Partially Supported by Polish Ministry of Science and Higher Education, grant DPN/N168/DESY/2009

<sup>f</sup> Supported by the Ministry of Education of the Czech Republic under the project INGO-LG14033

<sup>g</sup> Supported by the Swiss National Science Foundation

<sup>h</sup> Supported by CONACYT, México, grant 48778-F

<sup>i</sup> Russian Foundation for Basic Research (RFBR), Grant No. 1329.2008.2 and Rosatom

<sup>j</sup> Supported by the Romanian National Authority for Scientific Research under the contract PN 09370101

<sup>k</sup> Partially Supported by Ministry of Science of Montenegro, no. 05-1/3-3352

<sup>l</sup> Russian Foundation for Sciences, project no. 14-50-00150

<sup>m</sup> Ministry of Education and Science of Russian Federation contract no. 02.A03.21.0003.

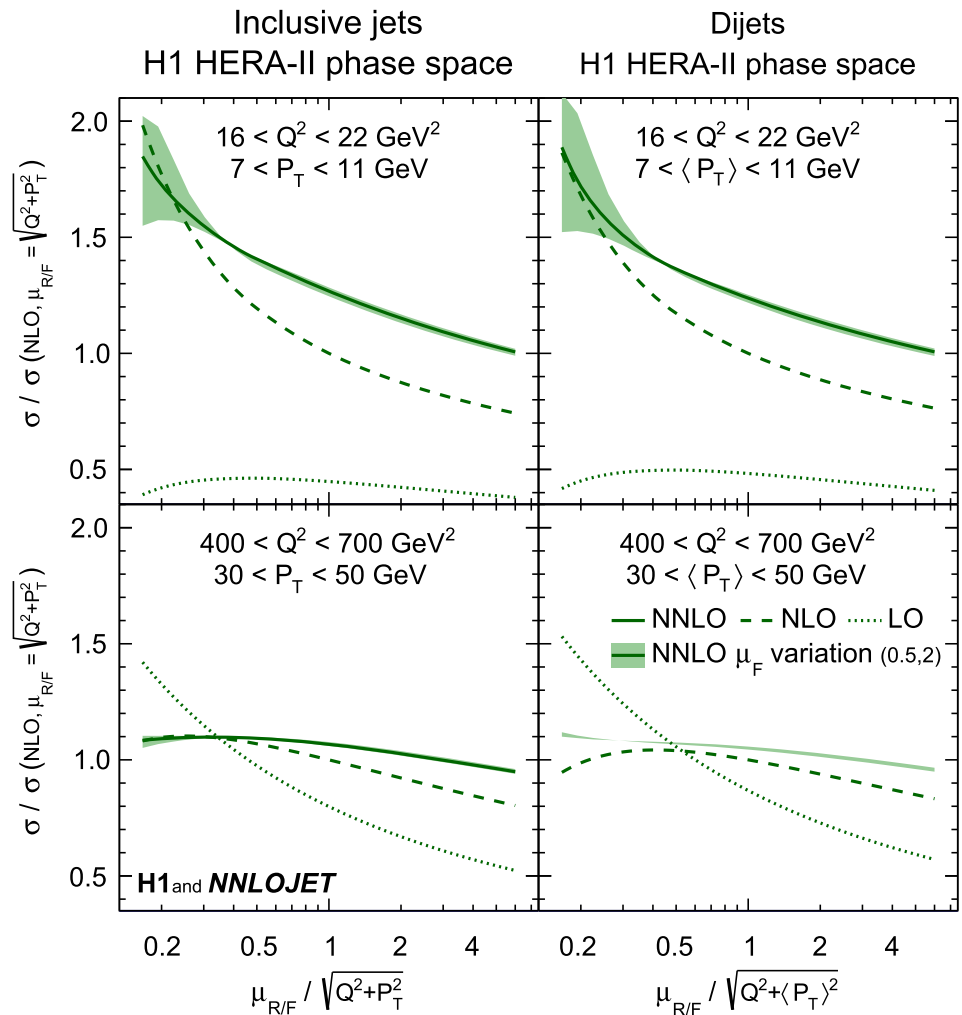
error in the NNLO predictions was found [4] which changes the numerical values of the predictions and the resulting values of the fits. Using the corrected NNLO predictions together with inclusive jet and dijet data, the strong coupling constant is determined to be  $\alpha_s(m_Z) = 0.1166 (19)_{\text{exp}} (24)_{\text{th}}$ . Complementarily,  $\alpha_s(m_Z)$  is determined together with parton distribution functions of the proton (PDFs) from jet and inclusive DIS data measured by the H1 experiment. The value  $\alpha_s(m_Z) = 0.1147 (25)_{\text{tot}}$  obtained is consistent with the determination from jet data alone. Corrected figures and numerical results are provided and the discussion is adapted accordingly.

**Erratum to: Eur. Phys. J. C (2017) 77:791**

<https://doi.org/10.1140/epjc/s10052-017-5314-7>

The determination of the strong coupling constant  $\alpha_s(m_Z)$  from H1 inclusive and dijet cross section data [1] exploits perturbative QCD predictions in next-to-next-to-leading order (NNLO) [2–4]. An implementation error of specific integrated initial-final antenna functions in the NNLO predictions that has impact on the numerical predictions for jet production cross sections in DIS was found in this numeric calculation [4]. This changes the values of the predictions and consequently the resulting values of the fits. The employed data cross sections and the  $\alpha_s$ -extraction methodology remain unchanged. In this erratum we provide corrections for two

**Fig. 1** Relative change of jet cross section as a function of a multiplicative factor applied to the renormalisation and factorisation scale for four exemplary data points of the HERA-II phase space. The bin definitions are displayed in the respective panels. The left panels show inclusive jet cross sections, and the right panels dijet cross sections. The full line shows the cross section dependence for the NNLO, the dashed line for NLO and the dotted line for LO calculations. For better comparison, all calculations are performed with the same PDF set (NNPDF3.1 NNLO). For all panels, the cross sections are normalised to the respective NLO cross section with unity scale factor. The filled area around the NNLO calculation indicates variations of the factorisation scale by factors of 0.5 and 2 around the chosen value for  $\mu_R$



tables of results and 16 corrected figures. The discussion is adjusted accordingly. Whereas numerical values quoted in the text are corrected, no change to the conclusions drawn is made. Further details are given in the original publication [1].

### 3 Determination of $\alpha_s(m_Z)$ from H1 jet cross sections

The strong coupling constant  $\alpha_s(m_Z)$  is determined from inclusive jet and dijet cross sections in NC DIS measured by the H1 collaboration and using NNLO QCD predictions. Fits are performed for each individual data set, for all inclusive jet measurements, for all dijet measurements, and for all H1 jet data taken together. The latter is denoted as ‘H1 jets’ in the following. In the case of fits to ‘H1 jets’, dijet data from the HERA-I running period however are excluded, since their statistical correlations to the respective inclusive jet data are not known.

For several studies, and to restrict the data to higher scales, a representative scale value  $\tilde{\mu}$  is assigned to each data point.

The value for  $\tilde{\mu}$  is calculated from the geometric mean of the bin boundaries in  $Q^2$  and  $P_T$  [1].

#### 3.1 Predictions

The inclusive jet and dijet NNLO predictions as a functions of the renormalisation scale  $\mu_R$  and the factorisation scale  $\mu_F$  are studied for selected phase space regions in Fig. 1. The dependence on the scale factor is strongest for cross sections at lower values  $\mu_R$ , i.e. lower values of  $Q^2$  and  $P_T$ . The NNLO predictions depend less on the scale factor than the NLO predictions.

#### 3.3 Sensitivity of the fit to input parameters

**Sensitivity to  $\alpha_s(m_Z)$**  The sensitivity of the data to  $\alpha_s(m_Z)$  and the consistency of the calculations are investigated by performing fits with two free parameters representing the two distinct appearances of  $\alpha_s(m_Z)$  in equation (1) of Ref. [1], i.e. in the PDF evolution,  $\alpha_s^\Gamma(m_Z)$ , and in the partonic cross

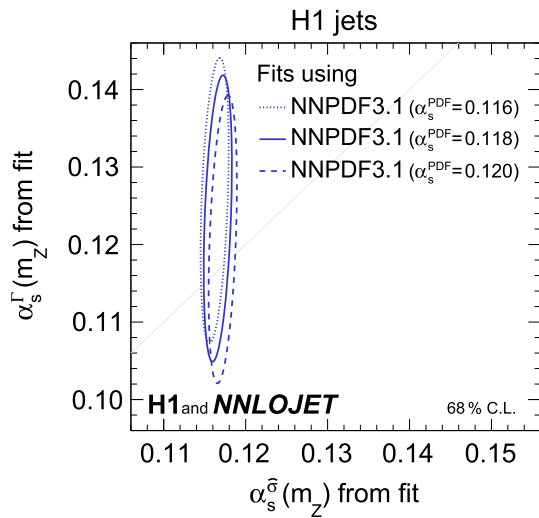


**Fig. 3** Results from fits to H1 jets with two free fit parameters for  $\alpha_s(m_Z)$ , where the appearances of  $\alpha_s(m_Z)$  in the PDF evolution  $\alpha_s^\Gamma(m_Z)$  and in the partonic cross sections  $\alpha_s^\sigma(m_Z)$  are identified separately. The ellipses display a confidence level of 68 % including the experimental, hadronisation and PDF uncertainties, and thus the lines are calculated for  $\Delta\chi^2 = 2.3$ . The dotted, full and dashed lines indicate the contour for  $\Delta\chi^2 = 2.3$  using three versions of the NNPDF3.1 set which were obtained using values for  $\alpha_s^{\text{PDF}}(m_Z)$  of 0.116, 0.118 and 0.120, respectively. The grey straight line corresponds to  $\alpha_s^\Gamma(m_Z) = \alpha_s^\sigma(m_Z)$

sections,  $\alpha_s^{\hat{\sigma}}(m_Z)$ . The result of such a fit performed for H1 jets is displayed in Fig. 3.

**Dependence on the choice of PDF** Values of  $\alpha_s(m_Z)$  are determined for various PDF sets and for alternative values  $\alpha_s^{\text{PDF}}(m_Z)$ . The results obtained using different PDFs are displayed in Fig. 4 for fits to inclusive jet and dijet cross sections, and in Fig. 5 for H1 jets.

In Fig. 5 (right) only H1 jets with  $\tilde{\mu} > 28 \text{ GeV}$  are used. The predictions using NNPDF3.1 [5], determined with  $\alpha_s^{\text{PDF}}(m_Z) = 0.118$ , provide a good description of the data with  $\chi^2/n_{\text{dof}}$  smaller than unity (Fig. 4), where  $n_{\text{dof}}$  denotes the number of data points minus one.

**Scale variants and comparison of NLO and NNLO predictions** The dependence of the results on  $\mu_R$  and  $\mu_F$  is studied by applying scale factors to the definition of  $\mu_R$  and  $\mu_F$ . The values of  $\alpha_s(m_Z)$  and  $\chi^2/n_{\text{dof}}$  resulting from the fits to inclusive jet and to dijet cross sections are displayed in Fig. 6 indicating that the standard choice for the scales (unity scale factor) yields good values of  $\chi^2/n_{\text{dof}}$ . Figure 7 displays the resulting  $\alpha_s(m_Z)$  for fits to H1 jets.

Alternative choices for  $\mu_R$  and  $\mu_F$  are investigated and the results for  $\alpha_s(m_Z)$  with values of  $\chi^2/n_{\text{dof}}$  are displayed in

**Fig. 4** Dependencies of the fitted values of  $\alpha_s(m_Z)$  on the input PDFs for separate fits of inclusive jet and dijet data. Shown are fits using the ABMP, CT14, HERAPDF2.0, MMHT and NNPDF3.1 PDF sets. For each case, the PDFs are available for different input values  $\alpha_s^{\text{PDF}}(m_Z)$  used for the PDF determination, and these values are displayed on the horizontal axis. The PDFs are available only for discrete values of  $\alpha_s^{\text{PDF}}(m_Z)$  and the results are connected by smooth lines. The lower panel displays the resulting values of  $\chi^2/n_{\text{dof}}$  of the fits

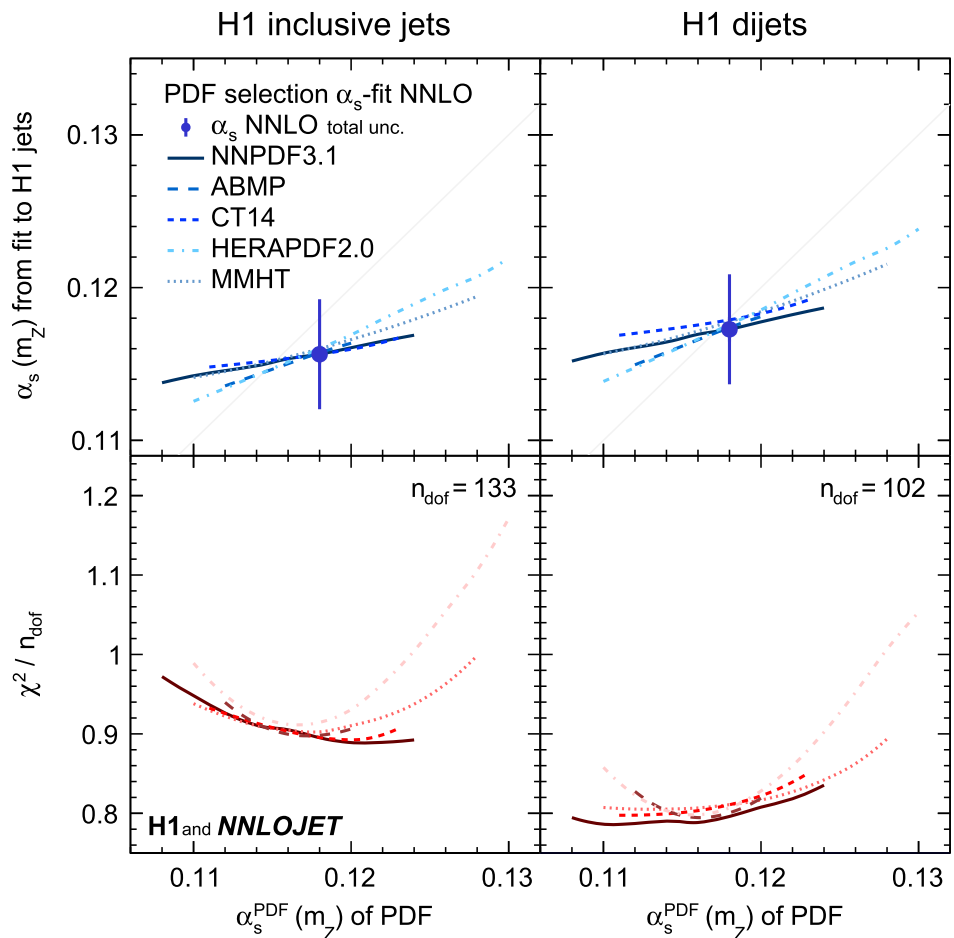


**Fig. 5** Dependencies of the fitted values of  $\alpha_s(m_Z)$  on the input PDFs for the H1 jets fit (left) and the H1 jets fit with  $\bar{\mu} > 28$  GeV (right). Further details are given in the caption of Fig. 4

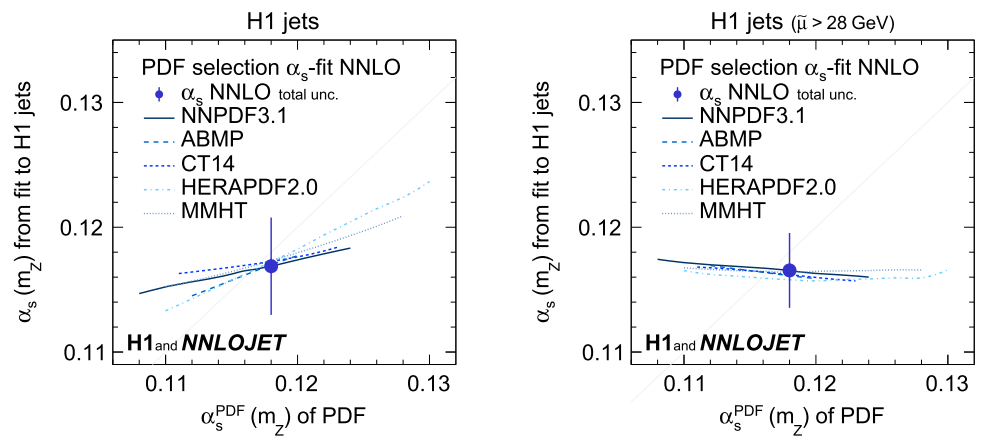


**Fig. 6** Dependencies of the fitted values of  $\alpha_s(m_Z)$  as a function of the scale factors applied to the renormalisation and factorisation scales ( $\mu_R$  and  $\mu_F$ ) for separate fits of inclusive jet and dijet data. The upper panels show the fitted value of  $\alpha_s(m_Z)$ , and the lower panels show the values of  $\chi^2/n_{dof}$ . The left (right) panels show the values for the fit to inclusive jet (dijet) cross sections. The solid lines show the effects from varying  $\mu_R$  and  $\mu_F$  together. The dashed (dotted) lines show the effects from varying  $\mu_R$  ( $\mu_F$ ) alone

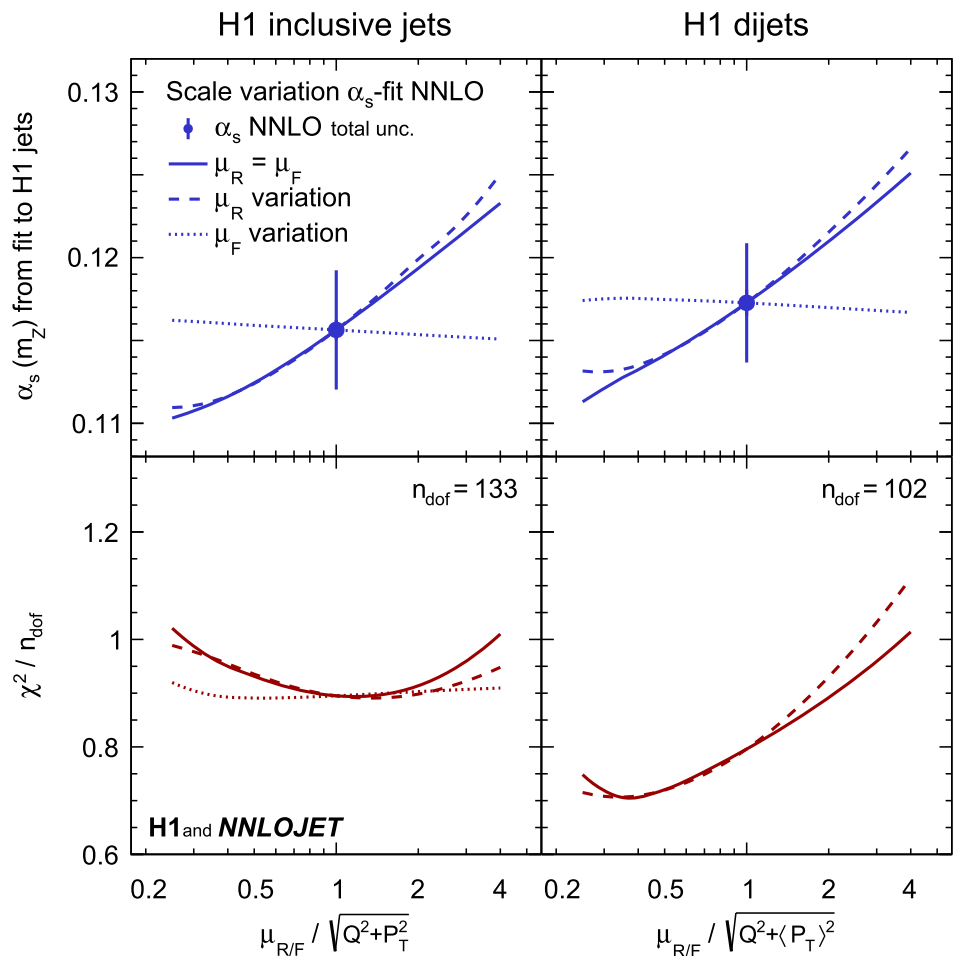


**Fig. 8** for fits to inclusive jet and dijet data. The nominal scale definition  $\mu_R^2 = \mu_F^2 = Q^2 + P_T^2$  results in good agreement of theory and data in terms of  $\chi^2/n_{dof}$ . The results obtained with alternative scale choices typically vary within the assigned scale uncertainty. This is also observed for fits to H1 jets, presented in Fig. 9.

The NLO calculations exhibit an enhanced sensitivity to the choice of the scale and to scale variations, as com-

pared to NNLO, resulting in scale uncertainties of  $\alpha_s(m_Z)$  of 0.0077, 0.0081 and 0.0083 for inclusive jets, dijet and H1 jets, respectively, as compared to uncertainties of 0.0034, 0.0033 and 0.0038 in NNLO, respectively. The previously observed reduction of scale uncertainties of the cross section predictions at NNLO [3,4,6] is reflected in a corresponding reduction of the  $\alpha_s(m_Z)$  scale uncertainties.

**Fig. 7** Dependencies of the fitted values of  $\alpha_s(m_Z)$  as a function of the scale factors for the H1 jets fit (left) and the H1 jets fit with  $\bar{\mu} > 28$  GeV (right). Further details are given in the caption of Fig. 6

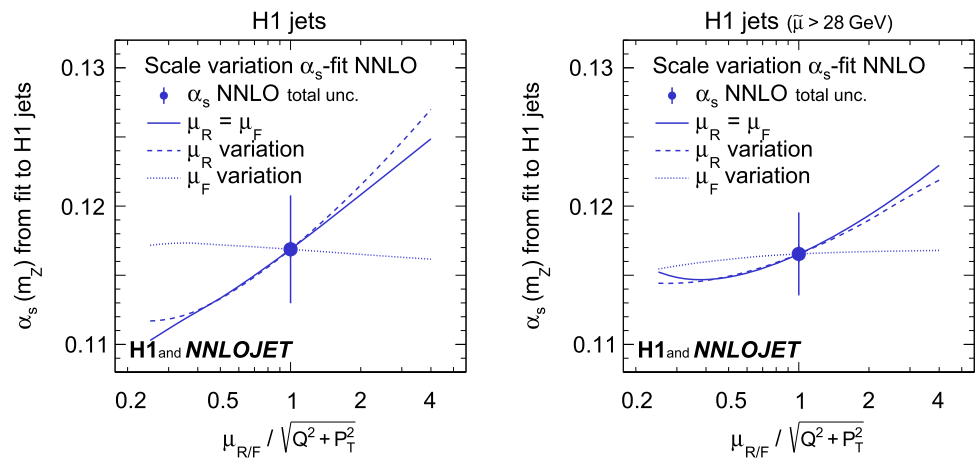


**Fig. 8** Values of  $\alpha_s(m_Z)$  obtained for different definitions of the renormalisation and factorisation scales ( $\mu_R$  and  $\mu_F$ ) in separate fits of inclusive jet and dijet data. The lower panels show  $\chi^2/n_{\text{dof}}$  of the fits. The open circles display results obtained using NLO matrix elements. The vertical bars indicate the scale uncertainties displayed together with the nominal scale choice

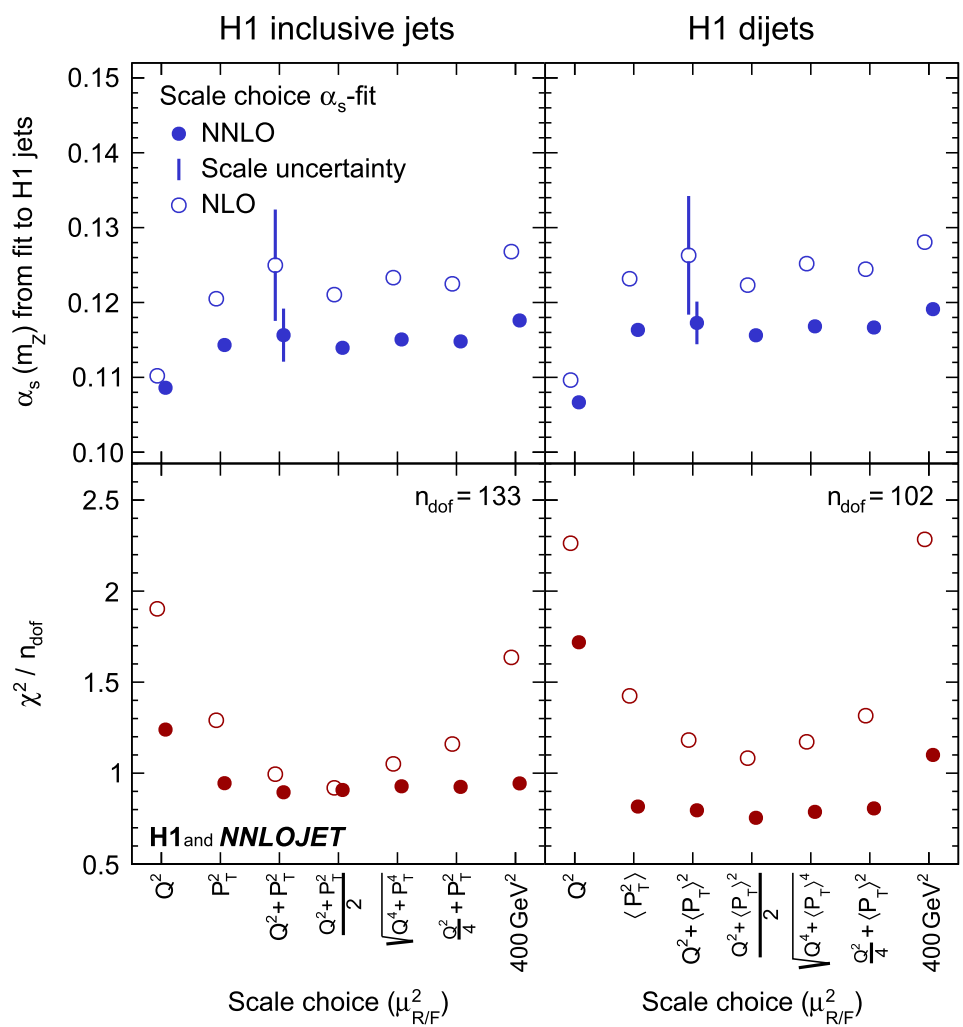


**Fig. 9** Values of  $\alpha_s(m_Z)$  obtained for different definitions of the renormalisation and factorisation scales ( $\mu_R$  and  $\mu_F$ ) in the H1 jets fit (left) and the H1 jets fit with  $\tilde{\mu} > 28$  GeV (right). The open circles display results obtained using NLO matrix elements. The vertical bars indicate the scale uncertainties displayed together with the nominal scale choice

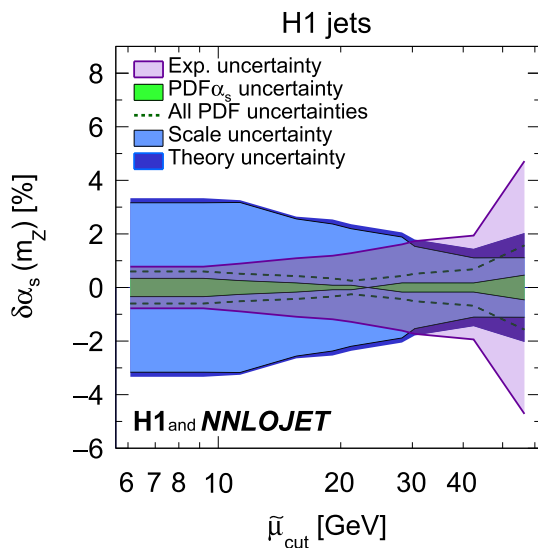
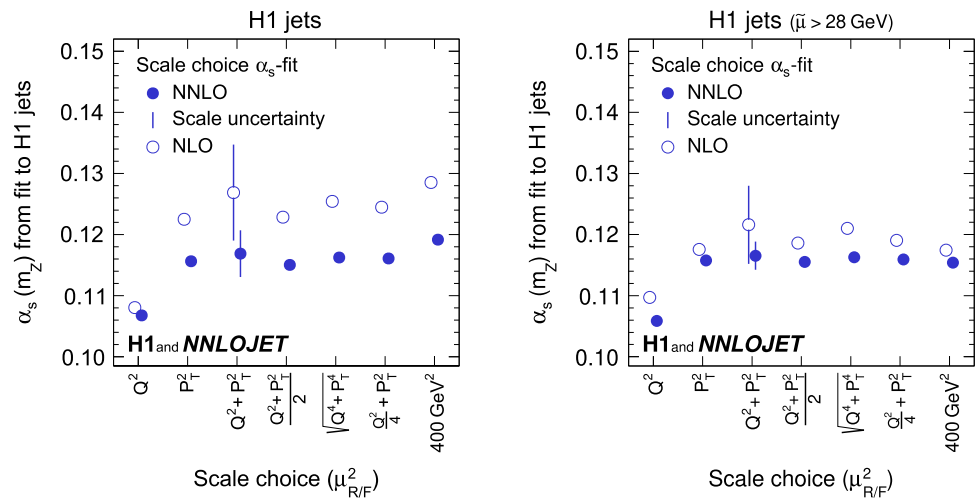


**Fig. 10** Uncertainties of the  $\alpha_s$  fit as a function of the parameter  $\tilde{\mu}_{\text{cut}}$  which restricts the jet data to high scales. The experimental, scale,  $\text{PDF}\alpha_s$ , quadratic sum of all PDF related uncertainties, and the theory uncertainty are shown

**Restricting the scale  $\tilde{\mu}$**  In order to study the size of the uncertainties as a function of  $\tilde{\mu}$ , the fits to inclusive jet and to dijet cross sections are repeated using only those data points exceeding a given value  $\tilde{\mu}_{\text{cut}}$ . The resulting uncertainties are displayed in Fig. 10.

3.4 Results

The values of  $\alpha_s(m_Z)$  obtained from the fits to the data are collected in Table 4 and displayed in Fig. 11. Good agreement between theory and data is found.

For the fits to the individual data sets the  $\chi^2/n_{\text{dof}}$  is below unity in most cases. The  $\alpha_s(m_Z)$  values are all found to be

consistent, in particular between inclusive jet and dijet measurements.

The fits to the inclusive jet data exhibit very reasonable  $\chi^2/n_{\text{dof}}$  values, thus indicating the consistency of the individual data sets. The value of  $\alpha_s(m_Z)$  from ‘H1 inclusive jets’ has a significantly reduced experimental uncertainty compared to the results for the individual data sets. The cut  $\tilde{\mu} > 28$  GeV results for inclusive jets in  $0.1158(19)_{\text{exp}}(23)_{\text{th}}$ , which is consistent with the world average [7,8].

Value of  $\chi^2/n_{\text{dof}}$  lower than unity are obtained for fits to all dijet cross sections confirming their consistency. The results agree with those from inclusive jet cross sections and the world average. At high scales  $\tilde{\mu} > 28$  GeV, a value  $\alpha_s(m_Z) = 0.1157(22)_{\text{exp}}(23)_{\text{th}}$  is found.

The fit to H1 jets yields  $\chi^2/n_{\text{dof}} = 0.87$  for 200 data points and  $\alpha_s(m_Z) = 0.1170(9)_{\text{exp}}(39)_{\text{th}}$ .

The  $\alpha_s(m_Z)$  value obtained from H1 jet data restricted to  $\tilde{\mu} > 28$  GeV is

$$\alpha_s(m_Z) = 0.1166(19)_{\text{exp}}(9)_{\text{had}}(3)_{\text{PDF}}(2)_{\text{PDF}\alpha_s}(4)_{\text{PDFset}}(21)_{\text{scale}}$$

with  $\chi^2 = 62.4$  for 91 data points.

In the present analysis, the value with the smallest total uncertainty is obtained in a fit to H1 jets restricted to  $\tilde{\mu} > 42$  GeV with the result  $\alpha_s(m_Z) = 0.1172(23)_{\text{exp}}(18)_{\text{theo}}$  and a value of  $\chi^2/n_{\text{dof}} = 37.0/40$ .

The ratio of all H1 jet cross section measurements to the NNLO predictions is displayed in Fig. 12. Overall good agreement between data and predictions is observed.

**Running of the strong coupling constant** The strong coupling is determined in fits to data points grouped into intervals  $[\tilde{\mu}_{\text{lo}}; \tilde{\mu}_{\text{up}}]$  of  $\tilde{\mu}$ . The results for fits to inclusive jet and to dijet cross sections, as well as to H1 jets, are presented for the ten selected intervals in  $\tilde{\mu}$  in Table 5 and are displayed

**Table 4** Summary of values of  $\alpha_s(m_Z)$  from fits to H1 jet cross section measurements using NNLO predictions. The uncertainties denote the experimental (exp), hadronisation (had), PDF, PDF $\alpha_s$ , PDFset and scale uncertainties as described in the text. The rightmost three columns denote the quadratic sum of the theoretical uncertainties (th), the total (tot) uncertainties and the value of  $\chi^2/n_{\text{dof}}$  of the corresponding fit. Along the vertical direction, the table data are segmented into five parts. The uppermost part summarises fits to individual inclusive jet datasets. The second part corresponds to fits of the individual dijet datasets. The

third part summarises fits to all inclusive jets or all dijets together, with different choices of the lower cut on the scale  $\tilde{\mu}_{\text{cut}}$ . The fourth group of fits, labelled H1 jets, is made using all available dijet and inclusive jet data together, for three different choices of  $\tilde{\mu}_{\text{cut}}$ . The bottom row corresponds to a combined fit of inclusive data and normalised jet data. For that fit, theoretical uncertainties related to the PDF determination interfere with the experimental uncertainties and overall theoretical uncertainty is quoted

$\alpha_s(m_Z)$ values from H1 jet cross sections					
Data	$\tilde{\mu}_{\text{cut}}$	$\alpha_s(m_Z)$ with uncertainties	th	tot	$\chi^2/n_{\text{dof}}$
<b>Inclusive jets</b>					
300 GeV high- $Q^2$	$2m_b$	0.1253 (33) <sub>exp</sub> (23) <sub>had</sub> (5) <sub>PDF</sub> (3) <sub>PDF<math>\alpha_s</math></sub> (5) <sub>PDFset</sub> (28) <sub>scale</sub>	(37) <sub>th</sub>	(49) <sub>tot</sub>	3.7/15
HERA-I low- $Q^2$	$2m_b$	0.1113 (18) <sub>exp</sub> (8) <sub>had</sub> (5) <sub>PDF</sub> (5) <sub>PDF<math>\alpha_s</math></sub> (7) <sub>PDFset</sub> (33) <sub>scale</sub>	(36) <sub>th</sub>	(40) <sub>tot</sub>	14.6/22
HERA-I high- $Q^2$	$2m_b$	0.1163 (26) <sub>exp</sub> (9) <sub>had</sub> (6) <sub>PDF</sub> (4) <sub>PDF<math>\alpha_s</math></sub> (3) <sub>PDFset</sub> (22) <sub>scale</sub>	(25) <sub>th</sub>	(36) <sub>tot</sub>	13.2/23
HERA-II low- $Q^2$	$2m_b$	0.1212 (16) <sub>exp</sub> (12) <sub>had</sub> (4) <sub>PDF</sub> (4) <sub>PDF<math>\alpha_s</math></sub> (3) <sub>PDFset</sub> (38) <sub>scale</sub>	(40) <sub>th</sub>	(43) <sub>tot</sub>	28.2/40
HERA-II high- $Q^2$	$2m_b$	0.1156 (20) <sub>exp</sub> (10) <sub>had</sub> (5) <sub>PDF</sub> (4) <sub>PDF<math>\alpha_s</math></sub> (2) <sub>PDFset</sub> (24) <sub>scale</sub>	(27) <sub>th</sub>	(34) <sub>tot</sub>	33.7/29
<b>Dijets</b>					
300 GeV high- $Q^2$	$2m_b$	0.1246 (41) <sub>exp</sub> (18) <sub>had</sub> (5) <sub>PDF</sub> (2) <sub>PDF<math>\alpha_s</math></sub> (3) <sub>PDFset</sub> (34) <sub>scale</sub>	(39) <sub>th</sub>	(57) <sub>tot</sub>	8.5/15
HERA-I low- $Q^2$	$2m_b$	0.1121 (24) <sub>exp</sub> (8) <sub>had</sub> (5) <sub>PDF</sub> (4) <sub>PDF<math>\alpha_s</math></sub> (5) <sub>PDFset</sub> (34) <sub>scale</sub>	(36) <sub>th</sub>	(44) <sub>tot</sub>	10.2/20
HERA-II low- $Q^2$	$2m_b$	0.1198 (12) <sub>exp</sub> (12) <sub>had</sub> (5) <sub>PDF</sub> (5) <sub>PDF<math>\alpha_s</math></sub> (3) <sub>PDFset</sub> (42) <sub>scale</sub>	(44) <sub>th</sub>	(45) <sub>tot</sub>	17.0/41
HERA-II high- $Q^2$	$2m_b$	0.1116 (22) <sub>exp</sub> (7) <sub>had</sub> (5) <sub>PDF</sub> (3) <sub>PDF<math>\alpha_s</math></sub> (3) <sub>PDFset</sub> (15) <sub>scale</sub>	(18) <sub>th</sub>	(29) <sub>tot</sub>	21.5/23
<b>Datasets combined</b>					
H1 inclusive jets	$2m_b$	0.1157 (10) <sub>exp</sub> (6) <sub>had</sub> (4) <sub>PDF</sub> (4) <sub>PDF<math>\alpha_s</math></sub> (2) <sub>PDFset</sub> (34) <sub>scale</sub>	(36) <sub>th</sub>	(37) <sub>tot</sub>	118.1/133
H1 inclusive jets	28 GeV	0.1158 (19) <sub>exp</sub> (9) <sub>had</sub> (2) <sub>PDF</sub> (2) <sub>PDF<math>\alpha_s</math></sub> (4) <sub>PDFset</sub> (21) <sub>scale</sub>	(23) <sub>th</sub>	(30) <sub>tot</sub>	43.0/60
H1 dijets	$2m_b$	0.1174 (11) <sub>exp</sub> (8) <sub>had</sub> (5) <sub>PDF</sub> (4) <sub>PDF<math>\alpha_s</math></sub> (3) <sub>PDFset</sub> (33) <sub>scale</sub>	(36) <sub>th</sub>	(38) <sub>tot</sub>	80.3/102
H1 dijets	28 GeV	0.1157 (22) <sub>exp</sub> (12) <sub>had</sub> (3) <sub>PDF</sub> (2) <sub>PDF<math>\alpha_s</math></sub> (3) <sub>PDFset</sub> (19) <sub>scale</sub>	(23) <sub>th</sub>	(32) <sub>tot</sub>	31.6/43
<b>All jet data combined</b>					
H1 jets	$2m_b$	0.1170 (9) <sub>exp</sub> (7) <sub>had</sub> (5) <sub>PDF</sub> (4) <sub>PDF<math>\alpha_s</math></sub> (2) <sub>PDFset</sub> (38) <sub>scale</sub>	(39) <sub>th</sub>	(40) <sub>tot</sub>	173.0/199
H1 jets	28 GeV	0.1166 (19) <sub>exp</sub> (9) <sub>had</sub> (3) <sub>PDF</sub> (2) <sub>PDF<math>\alpha_s</math></sub> (4) <sub>PDFset</sub> (21) <sub>scale</sub>	(24) <sub>th</sub>	(30) <sub>tot</sub>	62.4/90
H1 jets	42 GeV	0.1172 (23) <sub>exp</sub> (8) <sub>had</sub> (2) <sub>PDF</sub> (2) <sub>PDF<math>\alpha_s</math></sub> (7) <sub>PDFset</sub> (14) <sub>scale</sub>	(18) <sub>th</sub>	(29) <sub>tot</sub>	37.0/40
H1PDF2017[NNLO]	$2m_b$	0.1147 (11) <sub>exp,NP,PDF</sub> (2) <sub>mod</sub> (3) <sub>par</sub> (23) <sub>scale</sub>		(25) <sub>tot</sub>	1518.6/1516

in Fig. 13. Consistency is found for the fits to inclusive jets, dijets, and H1 jets, and the running of the strong coupling is confirmed in the accessible range of approximately 7 to 90 GeV.

The values obtained from fits to H1 jets are compared to other determinations of at least NNLO accuracy [9–12] and to results at NLO at very high scale [13] in Fig. 14, and consistency with the other experiments is found.

#### 4 Simultaneous $\alpha_s$ and PDF determination

In addition to the fits described above also a fit in NNLO accuracy of  $\alpha_s(m_Z)$  together with the non-perturbative PDFs is performed which takes jet data and inclusive DIS data as input. This fit is denoted as ‘PDF+ $\alpha_s$ -fit’ in the following.

#### 4.2 Results

**Fit results and the value of  $\alpha_s(m_Z)$**  The results of the PDF+ $\alpha_s$ -fit are presented in Table 6. The fit yields  $\chi^2/n_{\text{dof}} = 1518.6/(1529 - 13)$ , confirming good agreement between the predictions and the data. The resulting PDF is able to describe 141 jet data points and the inclusive DIS data simultaneously.

The value of  $\alpha_s(m_Z)$  is determined to

$$\alpha_s(m_Z) = 0.1147 (11)_{\text{exp,had,PDF}} (2)_{\text{mod}} (3)_{\text{par}} (23)_{\text{scale}},$$

and is determined to an overall precision of 2.2%. The  $\alpha_s(m_Z)$  value is consistent with the main result of the ‘H1 jets’ fit. The result is compared to values from the PDF fitting groups ABM [14], ABMP [15], BBG [16], HERAPDF [17], JR [18], NNPDF [19] and MMHT [20] in Fig. 15 and consistency is found. The result exhibits a competitive experimental uncertainty to other determinations [15, 19, 20], which is achieved



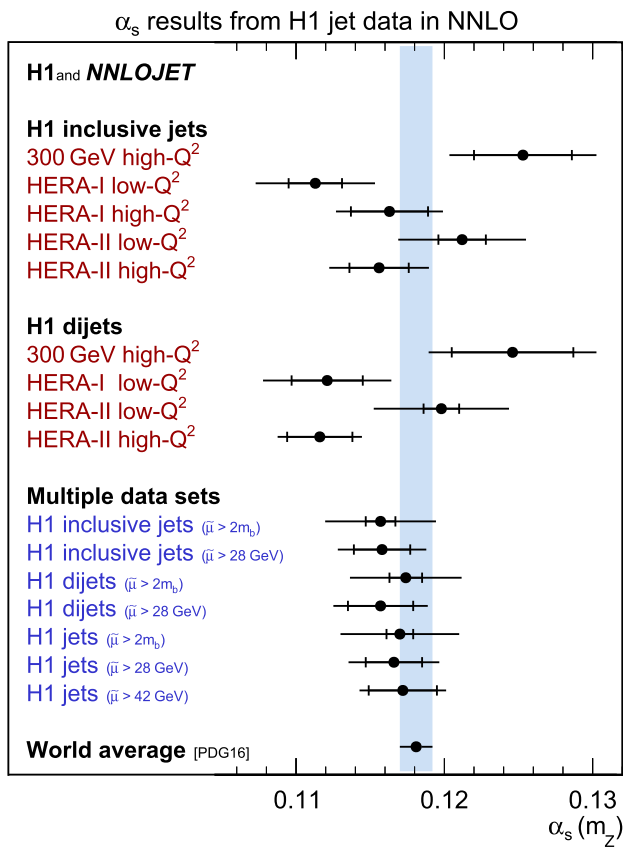


**Fig. 11** Summary of  $\alpha_s(m_Z)$  values obtained from fits to individual and multiple H1 jet data sets. The inner error bars indicate the experimental uncertainty and the outer error bars the total uncertainty

by using H1 normalised jet cross sections in addition to the H1 inclusive DIS data.

**PDF parametrisation results** The PDF and  $\alpha_s(m_Z)$  parameters determined together in this fit (Table 6) are denoted as H1PDF2017 [NNLO]. It is released [21] in the LHAPDF [22] format with experimental, hadronisation and  $\alpha_s(m_Z)$  uncertainties included. The gluon and singlet momentum distributions,  $xg$  and  $x\Sigma$ , the latter defined as the sum of all quark and anti-quark densities, are compared to NNPDF3.1 at a scale  $\mu_F = 20$  GeV in Fig. 16.

**The impact of H1 jet data on PDF fits** The PDF+ $\alpha_s$ -fit is repeated with the normalised jet data excluded, i.e. only inclusive DIS data are considered. The resulting Hessian error ellipses are displayed in Fig. 17 at a confidence level of 68%. Compared to the fit without jet data, the inclusion of jet data significantly reduces the uncertainties of  $\alpha_s(m_Z)$  and  $xg$ , as well as their correlation. The correlation coefficient is  $-0.92$  and reduce to  $-0.85$  if jet data is included.

## 5 Summary

The corrected new next-to-next-to-leading order pQCD calculations (NNLO) for jet production cross sections in neutral-current DIS are exploited for a determination of the strong coupling constant  $\alpha_s(m_Z)$  using inclusive jet and dijet cross section measurements published by the H1 collaboration. Two methods are explored to determine the value of  $\alpha_s(m_Z)$ .

In the first approach H1 inclusive jet and dijet data are analysed. The strong coupling constant is determined to be  $\alpha_s(m_Z) = 0.1166 (19)_{\text{exp}} (24)_{\text{th}}$ , where the jet data are restricted to high scales  $\tilde{\mu} > 28$  GeV. Uncertainties due to the input PDFs or the hadronisation corrections are found to be small, and the largest source of uncertainty is from scale variations of the NNLO calculations. The smallest total uncertainty on  $\alpha_s(m_Z)$  of 2.2% is obtained when restricting the data to  $\tilde{\mu} > 42$  GeV.

In a second approach a combined determination of PDF parameters and  $\alpha_s(m_Z)$  in NNLO accuracy is performed. In this fit all normalised inclusive jet and dijet cross sections published by H1 are analysed together with all inclusive neutral-current and charged-current DIS cross sections determined by H1. Using the data with  $Q^2 > 10$  GeV<sup>2</sup>, the value of  $\alpha_s(m_Z)$  is determined to be  $\alpha_s(m_Z) = 0.1147 (25)_{\text{tot}}$ . Consistency with the other results and the world average is found. The resulting PDF set H1PDF2017 [NNLO] is found to be consistent with the NNPDF3.1 PDF set at sufficiently large  $x > 0.01$ , albeit there are differences at lower  $x$ .

All jet cross section measurements are found to be well described by the NNLO predictions.

**Fig. 12** Ratio of inclusive jet (upper panel) and dijet cross sections (lower panel) to NNLO predictions obtained with the fitted value  $\alpha_s(m_Z) = 0.1157$ . Data points are ordered according to their scale  $\tilde{\mu}$  and are displayed on the horizontal axis within the respective  $\tilde{\mu}$ -interval. Within a single interval multiple data points are displayed with equal horizontal spacing and are thus not to scale. The displayed intervals reflect the choices made for the studies of the running of the strong coupling (compare Figs. 13 and 14). The shaded area indicates the uncertainty on the NNLO calculations from scale variations. The open circles show data points which are not considered for some fits, because their scale  $\tilde{\mu}$  is below  $2m_b$ . The squares show data points not considered for the ‘H1 jets’-fit, since the statistical correlations to the respective inclusive jet measurements are not known

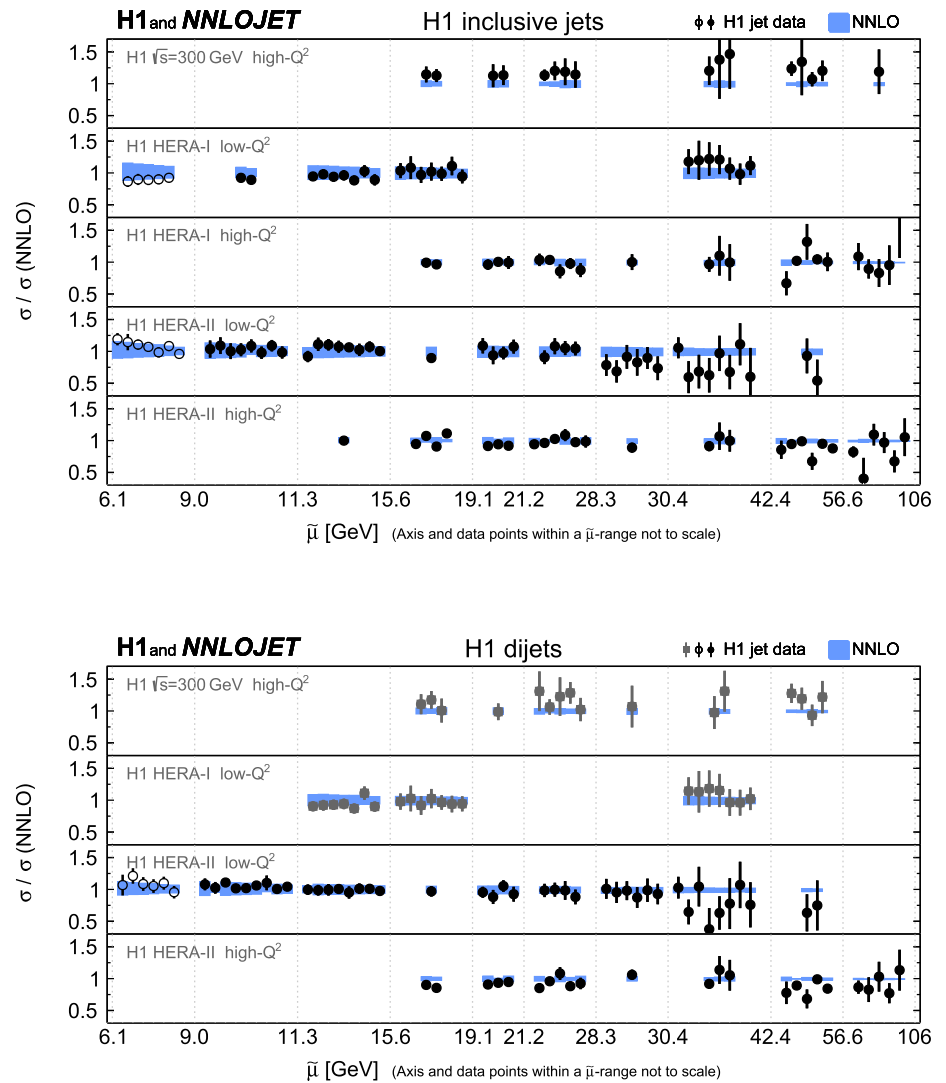


**Table 5** Values of the strong coupling constant  $\alpha_s(\mu_R)$  and at the Z-boson mass,  $\alpha_s(m_Z)$ , obtained from fits to groups of data points with comparable values of  $\mu_R$ . The first (second) uncertainty of each point

corresponds to the experimental (theory) uncertainty. The theory uncertainties include PDF related uncertainties and the dominating scale uncertainty

Running of the strong coupling						
$\mu_R$ [GeV]	Inclusive jets		Dijets		H1 jets	
	$\alpha_s(m_Z)$	$\alpha_s(\mu_R)$	$\alpha_s(m_Z)$	$\alpha_s(\mu_R)$	$\alpha_s(m_Z)$	$\alpha_s(\mu_R)$
7.4	0.1170 (12) (41)	0.1909 (33) (119)	0.1207 (25) (40)	0.1969 (70) (113)	0.1170 (12) (42)	0.1890 (33) (116)
10.1	0.1161 (17) (35)	0.1750 (40) (90)	0.1192 (14) (42)	0.1785 (32) (99)	0.1173 (13) (38)	0.1761 (30) (90)
13.3	0.1167 (15) (41)	0.1663 (31) (84)	0.1152 (18) (35)	0.1598 (36) (70)	0.1165 (15) (40)	0.1641 (31) (82)
17.2	0.1160 (15) (29)	0.1560 (28) (52)	0.1136 (19) (24)	0.1488 (33) (42)	0.1158 (16) (28)	0.1541 (29) (51)
20.1	0.1158 (18) (28)	0.1509 (31) (49)	0.1139 (21) (26)	0.1450 (35) (43)	0.1156 (17) (28)	0.1492 (29) (48)
24.5	0.1184 (16) (28)	0.1495 (26) (44)	0.1153 (22) (22)	0.1419 (34) (34)	0.1182 (17) (27)	0.1478 (27) (43)
29.3	0.1091 (32) (31)	0.1307 (47) (48)	0.1174 (26) (36)	0.1404 (38) (52)	0.1142 (25) (33)	0.1370 (37) (48)
36.0	0.1164 (27) (38)	0.1364 (38) (49)	0.1146 (31) (32)	0.1317 (41) (43)	0.1156 (26) (35)	0.1342 (35) (48)
49.0	0.1174 (22) (19)	0.1306 (27) (22)	0.1134 (31) (14)	0.1237 (37) (17)	0.1174 (23) (18)	0.1295 (28) (22)
77.5	0.1082 (51) (22)	0.1115 (54) (22)	0.1045 (77) (19)	0.1061 (80) (20)	0.1083 (51) (21)	0.1107 (53) (22)

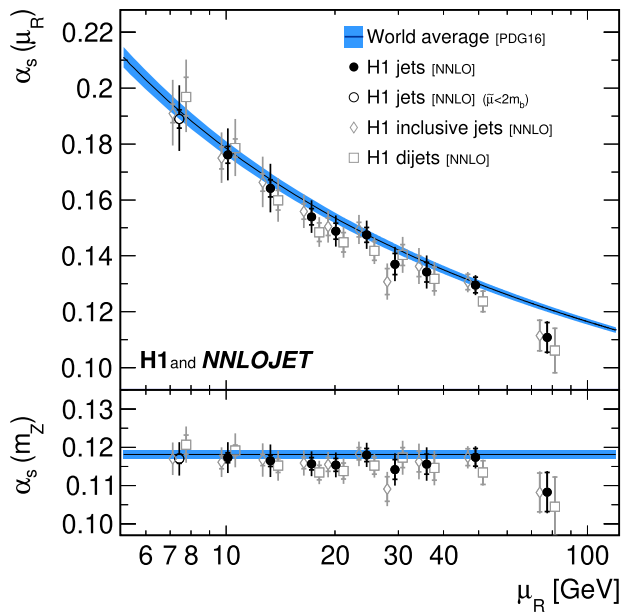


**Fig. 13** Results on  $\alpha_s(m_Z)$  and  $\alpha_s(\mu_R)$  for fits to data points arranged in groups of similar  $\mu_R$ . The circles show results from inclusive jet and dijet data taken together ('H1 jets'), the open diamonds results from inclusive jet cross sections alone and the open boxes results from dijet cross sections alone. For these fits, the data sets are not constrained by the requirement  $\tilde{\mu} > 2m_b$ . The fitted values of  $\alpha_s(m_Z)$  (lower panel) are translated to  $\alpha_s(\mu_R)$  (upper panel), using the solution of the QCD renormalisation group equation. The data points from fits to inclusive jets (dijets) are displaced to the left (right) for better visibility. In the upper panel a displacement is also applied along the vertical direction, to account for the running of  $\alpha_s(\mu_R)$ . The inner error bars denote the experimental uncertainties alone, and the outer error bars indicate the total uncertainties

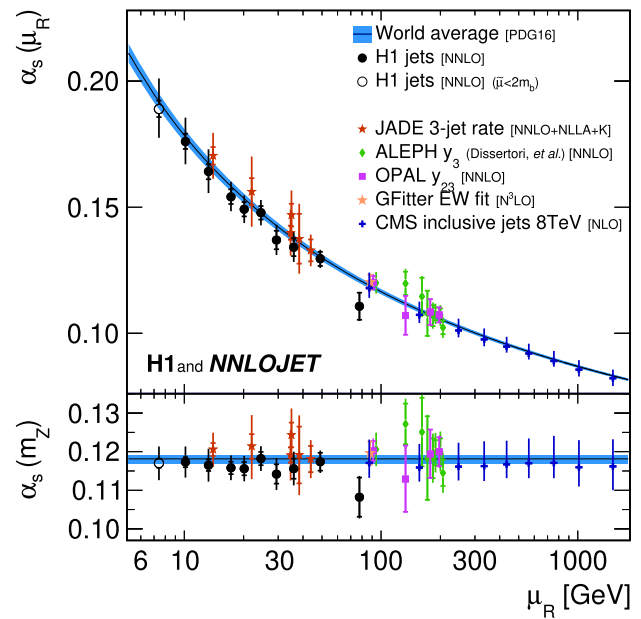


**Fig. 14** Results for  $\alpha_s(m_Z)$  and  $\alpha_s(\mu_R)$  for fits to data points arranged in groups of similar  $\mu_R$ , compared to results from other experiments and processes. Further details can be found in the caption of Fig. 13

**Table 6** Results of the PDF+ $\alpha_s$  fit. The columns denote the resulting fit value, its uncertainty and the correlations to the other parameters

Parameter	Fit result	Correlation coefficients												
		$\alpha_s(m_Z)$	$g_B$	$g_C$	$g_D$	$\tilde{u}_B$	$\tilde{u}_C$	$\tilde{u}_E$	$\tilde{d}_B$	$\tilde{d}_C$	$\tilde{U}_C$	$\tilde{D}_A$	$\tilde{D}_B$	$\tilde{D}_C$
$\alpha_s(m_Z)$	$0.1147 \pm 0.0011$	1												
$g_B$	$-0.030 \pm 0.029$	0.54	1											
$g_C$	$4.34 \pm 0.82$	0.08	0.49	1										
$g_D$	$-1.91 \pm 0.36$	0.30	0.25	0.81	1									
$\tilde{u}_B$	$0.721 \pm 0.025$	0.34	0.50	0.10	0.05	1								
$\tilde{u}_C$	$4.904 \pm 0.081$	-0.19	-0.20	-0.17	-0.16	-0.67	1							
$\tilde{u}_E$	$12.3 \pm 1.4$	0.04	-0.31	-0.23	-0.01	-0.10	0.62	1						
$\tilde{d}_B$	$1.032 \pm 0.080$	0.16	0.18	0.20	-0.11	0.22	-0.27	-0.11	1					
$\tilde{d}_C$	$5.27 \pm 0.44$	-0.13	0.00	-0.05	-0.04	-0.18	-0.22	0.03	0.80	1				
$\tilde{U}_C$	$4.51 \pm 0.50$	0.21	0.03	-0.04	0.09	0.61	0.07	-0.22	0.28	-0.04	1			
$\tilde{D}_A$	$0.268 \pm 0.016$	0.27	-0.41	-0.16	0.13	0.11	-0.01	0.10	0.11	-0.04	0.44	1		
$\tilde{D}_B$	$-0.107 \pm 0.010$	0.14	-0.59	-0.21	0.08	-0.08	0.02	0.18	-0.00	-0.07	0.29	0.91	1	
$\tilde{D}_C$	$13.09 \pm 0.22$	-0.18	-0.31	-0.41	-0.17	-0.12	-0.10	-0.07	0.20	0.26	-0.15	0.20	0.18	1
$g_A$	3.35	Constrained by sum-rules												
$\tilde{u}_A$	4.29	Constrained by sum-rules												
$\tilde{d}_A$	6.78	Constrained by sum-rules												
$\tilde{U}_A$	0.161	Set equal to $\tilde{D}_A(1 - f_s)$												
$\tilde{U}_B$	-0.107	Set equal to $\tilde{D}_B$												

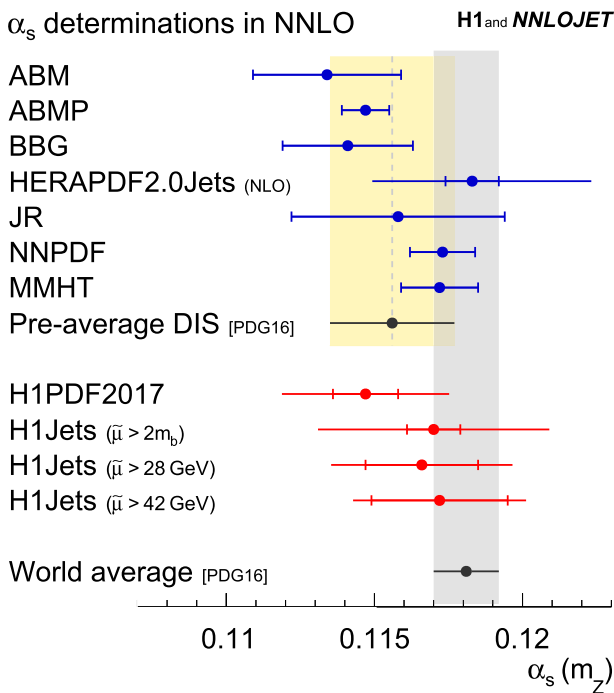


**Fig. 15** Comparison of the value of  $\alpha_s(m_Z)$  obtained in the H1PDF2017 [NNLO] PDF+ $\alpha_s$ -fit and in the H1 jets fit in NNLO accuracy to other  $\alpha_s$  determinations from DIS data. The pre-average of structure function data and the world average [8] are also indicated

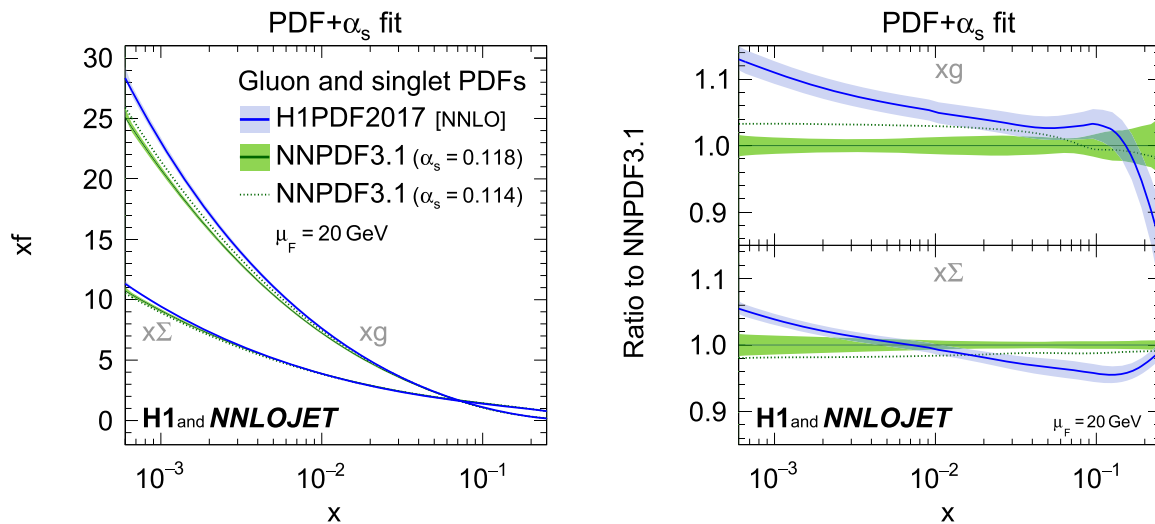


**Fig. 16** Gluon and singlet distributions determined by the PDF+ $\alpha_s$ -fit, denoted as H1PDF2017 [NNLO], as a function of the convolution variable  $x$ . The distributions are displayed at  $\mu_F = 20$  GeV. The PDFs are compared to the NNPDF3.1 PDFs determined with values of  $\alpha_s^{\text{PDF}}(m_Z)$  of 0.114 and 0.118. Ratios to NNPDF3.1 are shown in the right panels

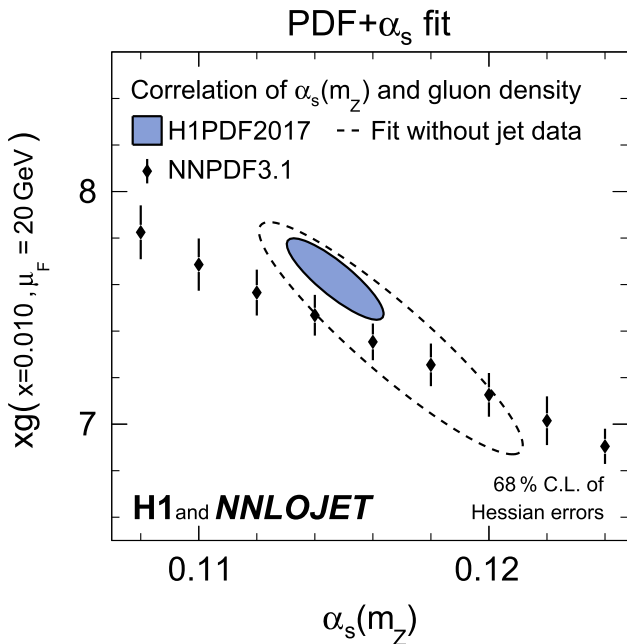


**Fig. 17** Error ellipses of Hessian uncertainties at 68% confidence level of  $\alpha_s(m_Z)$  and the gluon density  $xg$  at  $\mu_F = 20$  GeV and  $x = 0.01$  as a result of two different PDF+ $\alpha_s$ -fits. The filled ellipse indicates the result of the H1PDF2017 [NNLO] fit and the dashed line of a PDF+ $\alpha_s$ -fit with jet data excluded. The error ellipses represent the combined effect of experimental and hadronisation uncertainties as described in the text. The diamonds indicate the gluon density of the NNPDF3.1 PDF set for fixed values  $\alpha_s^{\text{PDF}}(m_Z)$

**Acknowledgements** We thank Robin Schürmann for performing independent re-derivations of integrated initial-final antenna functions, which have led to uncover the implementation error in the employed NNLO predictions.

**Open Access** This article is licensed under a Creative Commons Attribution 4.0 International License, which permits use, sharing, adaptation, distribution and reproduction in any medium or format, as long as you give appropriate credit to the original author(s) and the source, provide a link to the Creative Commons licence, and indicate if changes were made. The images or other third party material in this article are included in the article's Creative Commons licence, unless indicated otherwise in a credit line to the material. If material is not included in the article's Creative Commons licence and your intended use is not permitted by statutory regulation or exceeds the permitted use, you will need to obtain permission directly from the copyright holder. To view a copy of this licence, visit <http://creativecommons.org/licenses/by/4.0/>.  
Funded by SCOAP<sup>3</sup>.

**References**

1. H1 Collaboration, V. Andreev et al., Eur. Phys. J. C **77**, 791 (2017). <https://doi.org/10.1140/epjc/s10052-017-5314-7>. [arXiv:1709.07251](https://arxiv.org/abs/1709.07251)
2. A. Gehrmann-De Ridder, T. Gehrmann, E.W.N. Glover, A. Huss, T.A. Morgan, JHEP **1607**, 133 (2016). [https://doi.org/10.1007/JHEP07\(2016\)133](https://doi.org/10.1007/JHEP07(2016)133)

3. J. Currie, T. Gehrmann, J. Niehues, Phys. Rev. Lett. **117**, 042001 (2016). <https://doi.org/10.1103/PhysRevLett.117.042001>. arXiv:1606.03991
4. J. Currie, T. Gehrmann, A. Huss, J. Niehues, JHEP **1707**, 018, (2017). [https://doi.org/10.1007/JHEP07\(2017\)018](https://doi.org/10.1007/JHEP07(2017)018). arXiv:1703.05977. [Erratum: JHEP **2012**, 042 (2020)]
5. The NNPDF Collaboration, R.D. Ball et al., arXiv:1706.00428
6. H1 Collaboration, V. Andreev et al., Eur. Phys. J. C **77**, 215 (2017). <https://doi.org/10.1140/epjc/s10052-017-4717-9>. arXiv:1611.03421
7. S. Bethke, alpha s 2016, in *Proceedings, 19th International Conference in Quantum Chromodynamics (QCD 16): Montpellier, France, July 4–9, 2016*, vol. 282–284, p. 149 (2017). <https://doi.org/10.1016/j.nuclphysbps.2016.12.028>
8. Particle Data Group Collaboration, C. Patrignani et al., Chin. Phys. C **40**, 100001 (2016). <https://doi.org/10.1088/1674-1137/40/10/100001>
9. Gfitter Collaboration, M. Baak et al., Eur. Phys. J. C **74**, 3046 (2014). <https://doi.org/10.1140/epjc/s10052-014-3046-5>. arXiv:1407.3792
10. OPAL Collaboration, G. Abbiendi et al., Eur. Phys. J. C **71**, 1733 (2011). <https://doi.org/10.1140/epjc/s10052-011-1733-z>. arXiv:1101.1470
11. JADE Collaboration, J. Schieck, S. Bethke, S. Kluth, C. Pahl, Z. Trocsanyi, Eur. Phys. J. C **73**, 2332 (2013). <https://doi.org/10.1140/epjc/s10052-013-2332-y>. arXiv:1205.3714
12. G. Dissertori, A. Gehrmann-De Ridder, T. Gehrmann, E.W.N. Glover, G. Heinrich, H. Stenzel, JHEP **0802**, 040 (2008). <https://doi.org/10.1088/1126-6708/2008/02/040>. arXiv:0712.0327
13. CMS Collaboration, V. Khachatryan et al., JHEP **1703**, 156 (2017). [https://doi.org/10.1007/JHEP03\(2017\)156](https://doi.org/10.1007/JHEP03(2017)156). arXiv:1609.05331
14. S. Alekhin, J. Blümlein, S. Moch, Phys. Rev. D **86**, 054009 (2012). <https://doi.org/10.1103/PhysRevD.86.054009>. arXiv:1202.2281
15. S. Alekhin, J. Blümlein, S. Moch, R. Placakyte, arXiv:1701.05838
16. J. Blümlein, H. Böttcher, A. Guffanti, Nucl. Phys. B **774**, 182 (2007). <https://doi.org/10.1016/j.nuclphysb.2007.03.035>. arXiv:hep-ph/0607200
17. H1 and ZEUS Collaboration, H. Abramowicz et al., Eur. Phys. J. C **75**, 580 (2015). <https://doi.org/10.1140/epjc/s10052-015-3710-4>. arXiv:1506.06042
18. P. Jimenez-Delgado, E. Reya, Phys. Rev. D **79**, 074023 (2009). <https://doi.org/10.1103/PhysRevD.79.074023>. arXiv:0810.4274
19. R.D. Ball, V. Bertone, L. Del Debbio, S. Forte, A. Guffanti, J.I. Latorre, S. Lionetti, J. Rojo, M. Ubiali, Phys. Lett. B **707**, 66 (2012). <https://doi.org/10.1016/j.physletb.2011.11.053>. arXiv:1110.2483
20. L.A. Harland-Lang, A.D. Martin, P. Motylinski, R.S. Thorne, Eur. Phys. J. C **75**, 204 (2015). <https://doi.org/10.1140/epjc/s10052-015-3397-6>. arXiv:1412.3989
21. List of H1 publications, [https://www-h1.desy.de/publications/H1publication.short\\_list.html](https://www-h1.desy.de/publications/H1publication.short_list.html)
22. A. Buckley, J. Ferrando, S. Lloyd, K. Nordström, B. Page, M. Rüfenacht, M. Schönherr, G. Watt, Eur. Phys. J. C **75**, 132 (2015). <https://doi.org/10.1140/epjc/s10052-015-3318-8>. arXiv:1412.7420